U.S. DEPARTMENT OF ENERGY | Office of Science

DOE/SC-ARM-TR-336
PNNL-39349

Experimental Report: Multi-Instrument Comparison of AAF Condensation Particle Counters

F Mei MS Pekour

May 2026

ARM

DISCLAIMER

This report was prepared as an account of work sponsored by the U.S. Government. Neither the United States nor any agency thereof, nor any of their employees, makes any warranty, express or implied, or assumes any legal liability or responsibility for the accuracy, completeness, or usefulness of any information, apparatus, product, or process disclosed, or represents that its use would not infringe privately owned rights. Reference herein to any specific commercial product, process, or service by trade name, trademark, manufacturer, or otherwise, does not necessarily constitute or imply its endorsement, recommendation, or favoring by the U.S. Government or any agency thereof. The views and opinions of authors expressed herein do not necessarily state or reflect those of the U.S. Government or any agency thereof.

DOE/SC-ARM-TR-336
PNNL-39349

Experimental Report: Multi-Instrument Comparison of AAF Condensation Particle Counters

F Mei
MS Pekour
Both at Pacific Northwest National Laboratory

May 2026

How to cite this document:

Mei, F, and MS Pekour. 2026. Experimental Report: Multi-Instrument Comparison of AAF Condensation Particle Counters. U.S. Department of Energy, Atmospheric Radiation Measurement User Facility, Richland, Washington. DOE/SC-ARM-TR-336.

Work supported by the U.S. Department of Energy,
Office of Science, Office of Biological and Environmental Research

Acronyms and Abbreviations

AAF	ARM Aerial Facility
AE	aerosol electrometer
aMCPC	advanced mixing condensation particle counter
ARM	Atmospheric Radiation Measurement
CNC	condensation nucleus counter
CPC	condensation particle counter
DMA	differential mobility analyzer
FCE	Faraday cup electrometer
LOO	leave-one-out
MAE	mean absolute error
MBE	mean bias error
MCPC	mixing condensation particle counter
RMSE	root-mean-square error
SMPS	scanning mobility particle sizer
UCPC	ultrafine condensation particle counter

Contents

Acronyms and Abbreviations iii
1.0 Introduction 1
2.0 Instrument Description 1
3.0 Experimental Setup 2
3.1 Aerosol Generation and Conditioning 4
3.2 Reference Measurements 4
4.0 Data Analysis and Results 4
4.1 Overall Comparison of CPCs Against the Aerosol Electrometer 6
4.2 Leave-One-Out Averaged CPC Comparison for the Same Size Particles 7
4.3 Leave-One-Out Averaged CPC Comparison for the Different Size Particles 9
5.0 Summary 10
6.0 CPC Operation under Lower Pressures 11
6.1 Butanol-Based CPC Performance 11
6.2 Water-Based CPC Performance 13
7.0 Recommendations for Future Deployments 14
8.0 References 15

Figures

1 Experimental setup for CPC comparisons 3
2 Illustration of the CPC comparison setup 3
3 The total number concentrations measured by all nine CPCs versus the aerosol electrometer-inferred concentrations for the same-size, monodisperse aerosol tests 5
4 Time series plot of all CPCs and AE tested on March 10, 2026 6
5 The total number concentrations measured by eight CPCs versus the aerosol electrometer-inferred concentrations for the same-size, monodisperse aerosol tests 7
6 Leave-one-out averaged CPC comparison for the aerosol particles with the same size 8
7 Leave-one-out averaged CPC comparison for the aerosol particles with different sizes 9
8 Figure 3 from Bauer's paper: Counting efficiency curves (a: Grimm 5410 CEN and b: TSI 3772 CEN) as a function of the mobility diameter 12

Tables

1 Summary of CPC specifications....2
2 Linear regression results—All CPCs versus aerosol electrometer....4
3 Statistical performance metrics of various CPCs referenced to the aerosol electrometer....6
4 Side-by-side comparison of LOO regression parameters—same size versus different sizes....10
5 Table 2 from Bauer's paper: Results of the fits from Figures 2 and 3 for the different CPC models and pressure stages....12
6 Approximate plateau efficiency of TSI 3789 (7 nm mode) versus pressure with near-optimized conditioner temperature (same initiator and moderator temperatures, 59°C, 10 °C)....14

1.0 Introduction

Condensation particle counters (CPCs), also known as condensation nucleus counters (CNCs) are sophisticated instruments designed to measure the concentration of aerosol particles in the atmosphere. These devices are pivotal in environmental monitoring, industrial applications, and scientific research, particularly in atmospheric studies. CPCs are vital for understanding the role of aerosols in climate systems. Aerosols influence cloud formation, radiative forcing, and atmospheric chemistry. By providing accurate measurements of particle concentrations and distributions, CPCs contribute to models that predict atmospheric impact and weather patterns (Mei et al. 2021). CPCs operate by enlarging submicron particles, including those as small as a few nanometers, to sizes detectable by optical methods. This report delves into the mechanisms, importance, and contributions of CPCs to atmospheric research at the U.S. Department of Energy Atmospheric Radiation Measurement (ARM) Aerial Facility (AAF), highlighting their role in advancing air quality assessment, pollution control, and atmospheric studies.

2.0 Instrument Description

CPCs work by exposing aerosol particles to a supersaturated vapor, typically water or alcohol-based. The particles act as nucleation centers, leading to the condensation of the vapor into droplets. These droplets grow to approximately 10 µm in diameter, making them large enough to be detected and counted using optical scattering techniques (Chen and Pui 1995, Stolzenburg and McMurry 1991). The supersaturation process is diffusion-limited, ensuring uniform droplet sizes regardless of the original particle composition or dispersity. This characteristic allows CPCs to measure total particle concentrations without classifying them into size bins, making them ideal for applications requiring high sensitivity and broad detection ranges (Mei et al. 2021). Modern CPCs can detect particles as small as sub-3 nm and as large as 3 µm, with concentration measurements reaching up to 100,000 particles per cubic centimeter. They provide real-time readings with temporal resolutions as fine as in sub-second, enabling precise monitoring of dynamic aerosol environments (Kerminen et al. 2018).

The instruments included in this comparison study represent a range of designs, working fluids, and detection capabilities from three manufacturers. A total of nine CPCs were evaluated: three TSI CPC 3772, two TSI CPC 3789, one TSI CPC 3025, two Magic CPCs from Aerosol Dynamics Inc., and one Brechtel advanced Mixing CPC (aMCPC).(Bian et al. 2020, Hering et al. 2019, Kangasluoma and Attoui 2019, Kangasluoma et al. 2017, Mei et al. 2021)

The TSI CPC 3772 is a general-purpose, butanol-based CPC with a 50% counting efficiency (D50) cut size of approximately 10 nm. It is a robust and widely deployed instrument suitable for routine ambient aerosol monitoring. The TSI CPC 3789, also known as the versatile water-based CPC, replaces butanol with water as its working fluid and features a tunable D50 cut size ranging from approximately 2 nm to 7 nm, offering flexibility across a range of measurement applications. The TSI CPC 3025 is a well-established ultrafine CPC (UCPC) with a D50 of approximately 3 nm, making it one of the most sensitive instruments for detecting freshly nucleated particles; it has long served as a reference standard in intercomparison studies.

The Magic CPC, developed by Aerosol Dynamics Inc., employs a water-based, three-stage growth tube design (moderator, initiator, and growth region) that activates particles under gentle supersaturation

conditions, avoiding the need for butanol. The Brechtel MCPC uses a mixing-type condensation approach, combining warm saturated and cool unsaturated airflows to generate supersaturation. Its compact, lightweight design and tolerance to varying pressures make it particularly well-suited for aircraft deployments and operations at different altitudes.

The key specifications of each instrument are summarized in Table 1.

Table 1. Summary of CPC specifications.

Feature	TSI CPC 3772	TSI CPC 3789	TSI CPC 3025	Magic CPC (Aerosol Dynamics)	Brechtel MCPC
Working Fluid	Butanol	Water	Butanol	Water	Butanol
D50 Cut Size	~10 nm	~2–7 nm (tunable)	~3 nm	~5 nm (varies by model)	~10 nm
Sample Flow Rate	1.0 L/min	0.3–1.5 L/min	1.5 L/min	0.3 L/min	0.36 L/min
Max Concentration	~10^4 cm^{-3}	~2×10^5 cm^{-3}	~10^5 cm^{-3}	~2×10^5 cm^{-3}	~10^5 cm^{-3}
Condensation Method	Conductive cooling	Three-stage (conditioner, initiator, moderator)	Conductive cooling	Three-stage (moderator, initiator, growth)	Mixing (warm saturated + cool unsaturated air)
Typical Use	General ambient monitoring	Versatile lab and field use	Ultrafine particle detection; reference standard	Clean, water-based detection; field campaigns	field deployments
Key Advantage	Robust, simple operation, pressure-tolerant	Tunable cut size; no butanol, pressure-tolerant	Very low detection limit (~3 nm), pressure-tolerant	No butanol; gentle activation conditions	Compact, lightweight, pressure-tolerant
Key Limitation	Higher cut size (~10 nm)	Requires water management	Discontinued by manufacturer	Newer technology; less field heritage	Less common in standard lab settings
Number in Your Study	3	2	1	2	1

3.0 Experimental Setup

The experimental setup used in this intercomparison study is illustrated in Figures 1 and 2. The system was designed to deliver a well-characterized, monodisperse aerosol simultaneously to all instruments under test, ensuring a fair and consistent comparison of number concentration measurements.

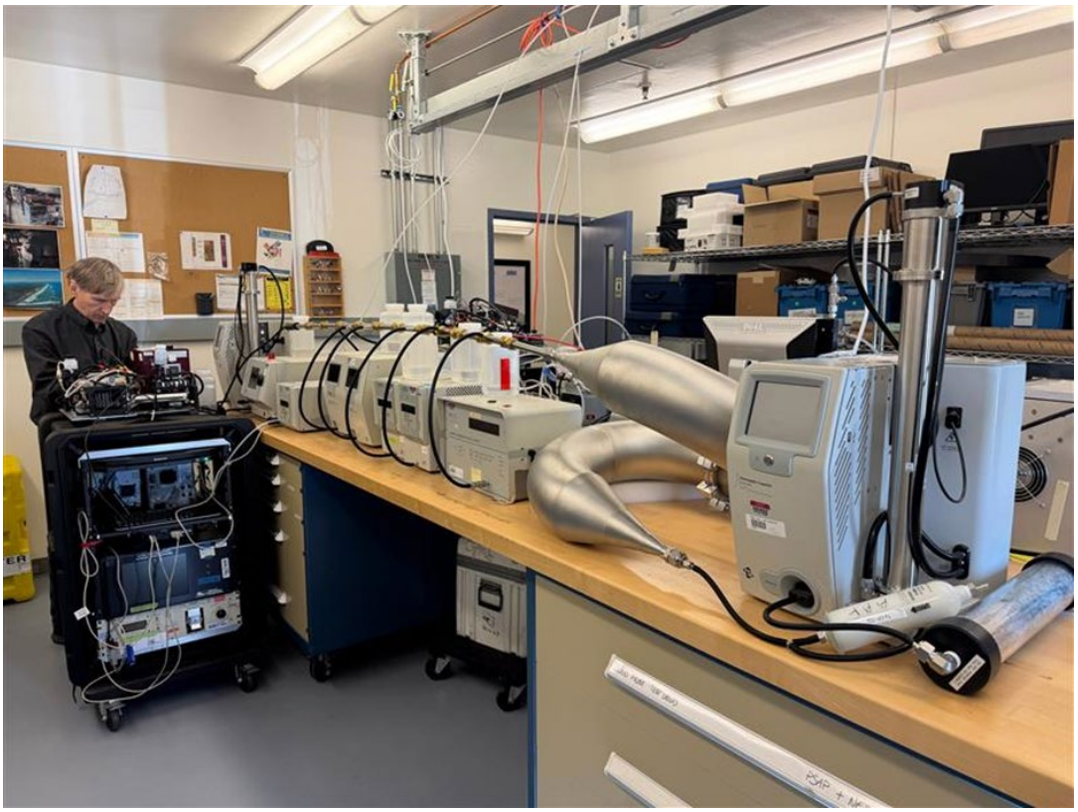


Figure 1. Experimental setup for CPC comparisons.

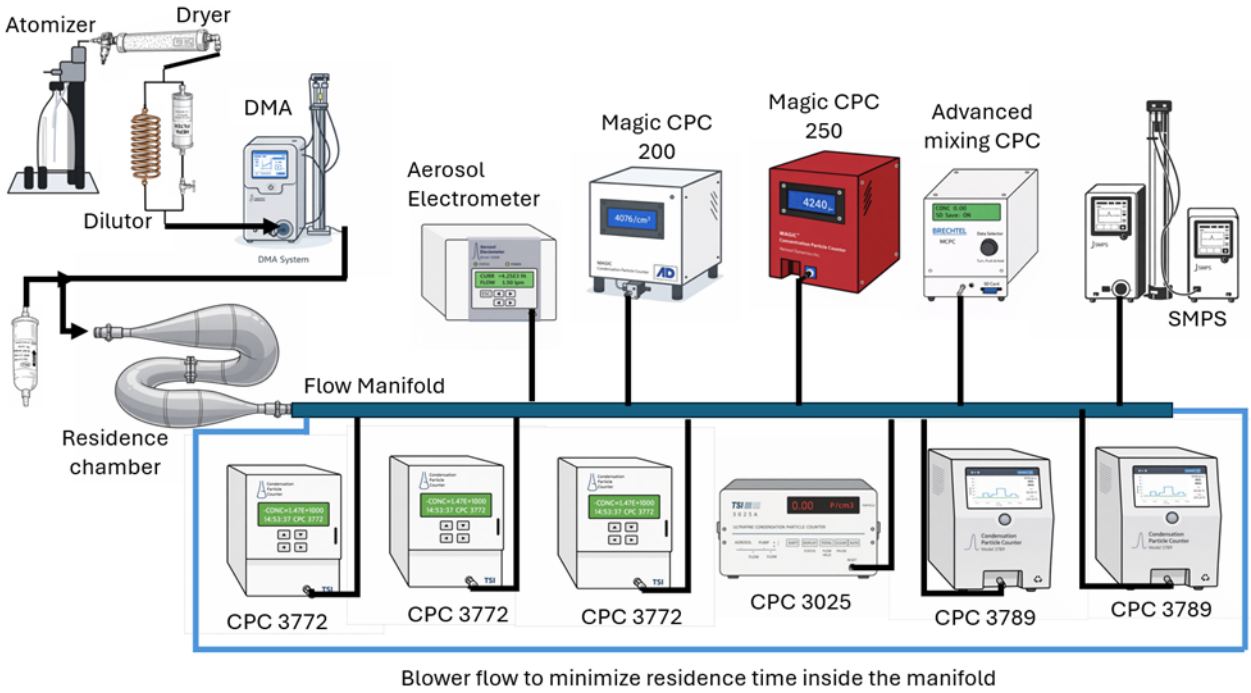


Figure 2. Illustration of the CPC comparison setup.

3.1 Aerosol Generation and Conditioning

Polydisperse aerosol particles were generated using an atomizer. The air was "pushed" through the atomizer to ensure delivery of polydisperse aerosol to a differential mobility analyzer (DMA) at specific flow rate. The output of the atomizer was dried and passed through a diluter before it was directed into the DMA, which selected particles of a specific electrical mobility diameter, producing a monodisperse aerosol stream. The size-selected aerosol was then passed through a residence chamber to allow the flow to stabilize and the particle concentration to become spatially uniform before reaching the instruments.

The conditioned aerosol exiting the residence chamber was introduced into a common sampling manifold (a ¾- inch tubing with multiple pickup points along the sampling line). This manifold was designed to evenly distribute the aerosol to all instruments simultaneously, minimizing concentration gradients and particle losses across the sampling ports. An additional blower was installed to circulate air through the manifold and back to the residence chamber, thereby improving mixing and minimizing time delays in the manifold.

3.2 Reference Measurements

The aerosol electrometer (TSI 3068B) provided a primary, charge-based measurement of particle number concentration, independent of optical detection. This served as an absolute reference against which all CPCs were compared. Additionally, the scanning mobility particle sizer (SMPS) was used to confirm the size and monodispersity of the DMA-selected aerosol throughout the experiment. Note that all the DMAs in this study were equipped with the TSI x-ray chargers.

4.0 Data Analysis and Results

Figure 3 presents the scatter plot of number concentrations measured by all nine CPCs versus the aerosol electrometer (AE) reference for the same-size, monodisperse aerosol tests. The data were collected from four days (March 10, March 11, March 16, and March 17, 2026). Each data point represents a simultaneous measurement (~1 Hz), and individual linear regression fits are shown for each instrument alongside the 1:1 reference line. A summary of the regression parameters is provided in Table 2.

Table 2. Linear regression results—All CPCs versus aerosol electrometer.

Instrument	Slope	Intercept (cm^{-3})	R^2
CPC 3025	0.86	546.2	0.98
CPC 3772a	0.762	454.9	0.982
CPC 3772b	0.767	489.2	0.979
CPC 3772c	0.751	440.4	0.983
CPC 3789a	0.8	472.4	0.983
CPC 3789b	0.793	472.9	0.982

Instrument	Slope	Intercept (cm^{-3})	R^2
Brechtel MCPC 28	0.937	961	0.889
Magic CPC (wcpc uas)	0.762	427.5	0.982
Magic CPC (wcpc uas backup)	0.736	333.8	0.977
All instruments combined	0.783	468.5	0.9533

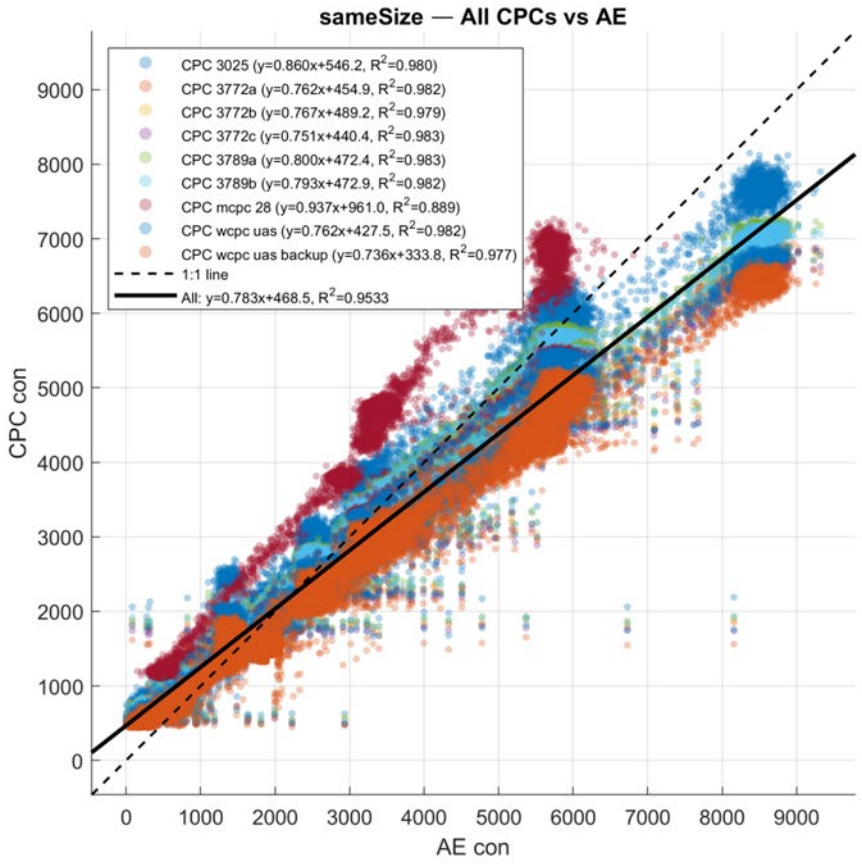


Figure 3. The total number concentrations measured by all nine CPCs versus the aerosol electrometer-inferred concentrations for the same-size, monodisperse aerosol tests.

All nine CPCs demonstrated a strong linear relationship with the aerosol electrometer, with R^2 values exceeding 0.977 for eight of the nine instruments and an overall combined R^2 of 0.9533. However, all CPCs measured lower concentrations than the AE, as evidenced by regression slopes consistently below 1.0. This systematic undercounting is a well-known characteristic in CPC-to-electrometer comparisons and may be attributed to differences in counting efficiency, charge-to-particle ratio estimation, particle losses in sampling lines, and the inherent measurement principles of each instrument.

The Brechtel aMCPC exhibited the largest intercept (961.0 cm^{-3}) and the lowest R^2 (0.889), indicating greater scatter in its measurements compared to the other instruments. This is due to the unstable

performance of the aMCPC during the testing. As shown in Figure 4, during testing on March 10, 2026, the instrument was flooded midway through, resulting in a data issue after 17:25. This issue repeated after cleaning the optical chamber. Thus, we decided to focus on the remaining eight CPCs for further discussion. To provide a clearer assessment of the remaining instruments, the aMCPC was removed from the analysis, and the data were replotted.

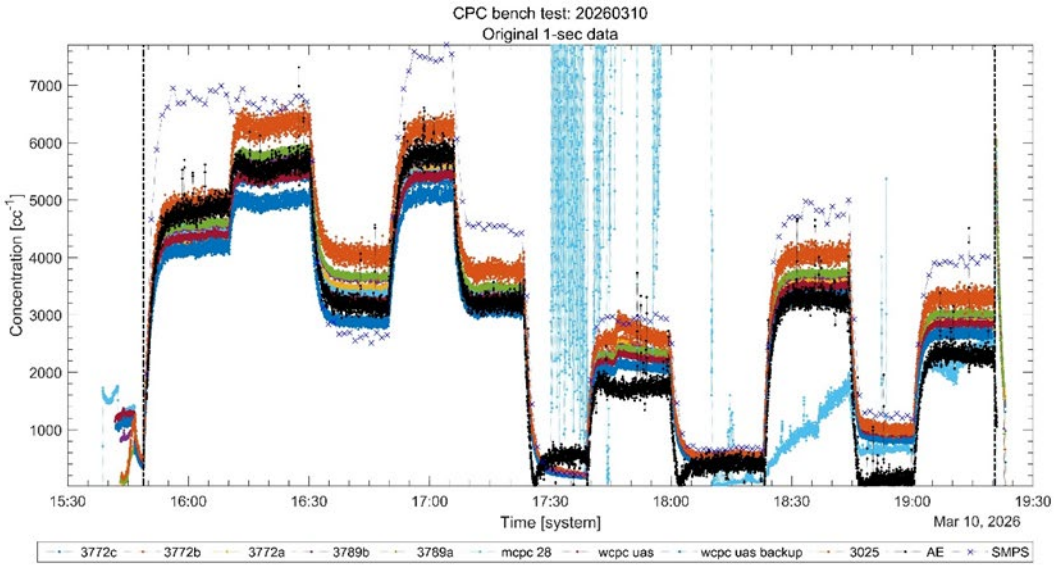


Figure 4. Time series plot of all CPCs and AE tested on March 10, 2026.

4.1 Overall Comparison of CPCs Against the Aerosol Electrometer

Figure 5 presents the revised scatter plot of number concentrations measured by the eight remaining CPCs versus the AE for same-size, monodisperse aerosol tests. The removal of the aMCPC resulted in a noticeably improved overall fit, with the combined regression improving from $R^2 = 0.9533$ to $R^2 = 0.9669$, and a slightly adjusted combined slope and intercept of $y = 0.779x + 453.7$. The individual regression parameters for each instrument are summarized in Table 3. Note that MAE is the mean absolute error. MBE is the mean bias error, and RMSE is the root-mean-square error.

Table 3. Statistical performance metrics of various CPCs referenced to the aerosol electrometer.

CPC_ID	N	Slope	Intercept	R^2	MAE	MBE	RMSE
3025	37639	0.8604	546.21	0.97988	296.94	77.08	381.46
3772a	35570	0.7624	454.91	0.9817	458.25	-343.66	623.68
3772b	35568	0.7665	489.18	0.97948	427.48	-295.58	596.85
3772c	35569	0.7505	440.42	0.98259	496.97	-398.19	670.28
3789a	35570	0.8004	472.42	0.98251	357.06	-198.53	495.7

CPC_ID	N	Slope	Intercept	R^2	MAE	MBE	RMSE
3789b	35565	0.7926	472.88	0.98238	374.22	-224.3	518.52
mcpc 28	7799	0.9365	960.96	0.88938	821.41	738.32	924.73
wcpc uas	35378	0.7621	427.46	0.98235	456.25	-350.96	622.23
wcpc uas backup	37640	0.7362	333.84	0.97731	616.82	-552.77	797.61

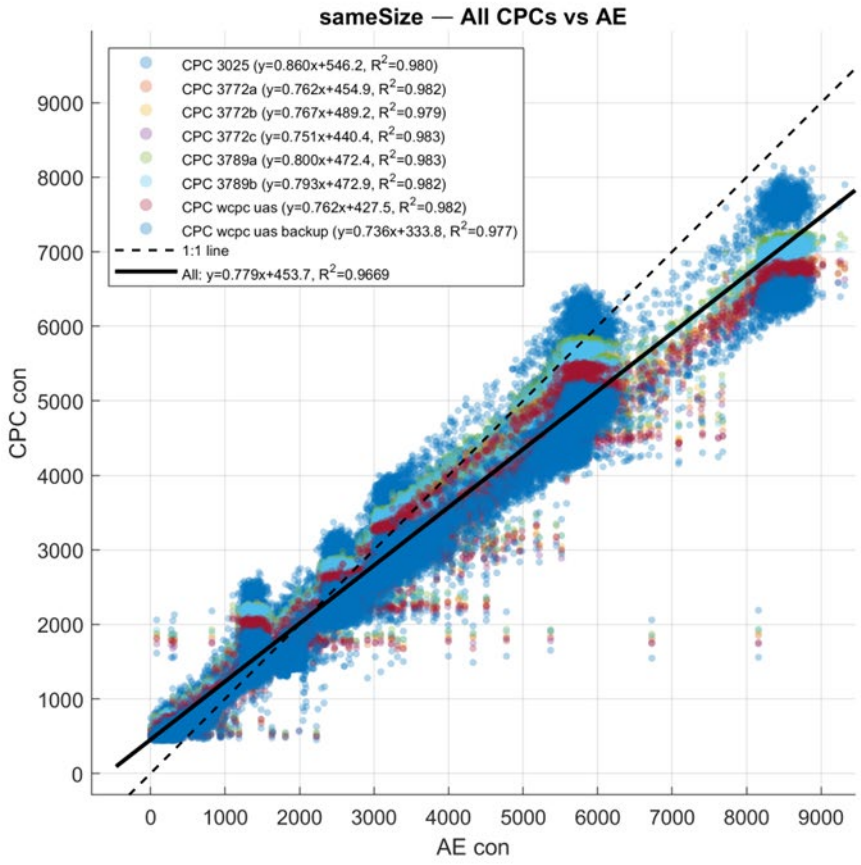


Figure 5. The total number concentrations measured by eight CPCs versus the aerosol electrometer-inferred concentrations for the same-size, monodisperse aerosol tests.

4.2 Leave-One-Out Averaged CPC Comparison for the Same Size Particles

In the previous analysis (Section 4.1), all eight CPCs consistently undercounted relative to the aerosol electrometer (AE), with slopes ranging from 0.736 to 0.860. This systematic undercounting suggests that the AE-inferred concentrations may be biased high due to the presence of multiply charged particles in the DMA-selected aerosol (100 nm). Since the AE measures total electrical current and assumes all particles carry a single charge, the presence of doubly or triply charged larger particles would cause the AE to overestimate the true number concentration.

To remove this bias and provide a more representative reference, we adopted a leave-one-out (LOO) averaging approach: for each CPC, the reference concentration was calculated as the mean of the remaining seven CPCs. This method ensures that no instrument is compared with itself and provides a CPC-consensus reference independent of the AE charge assumption. The results are presented in Figure 6.

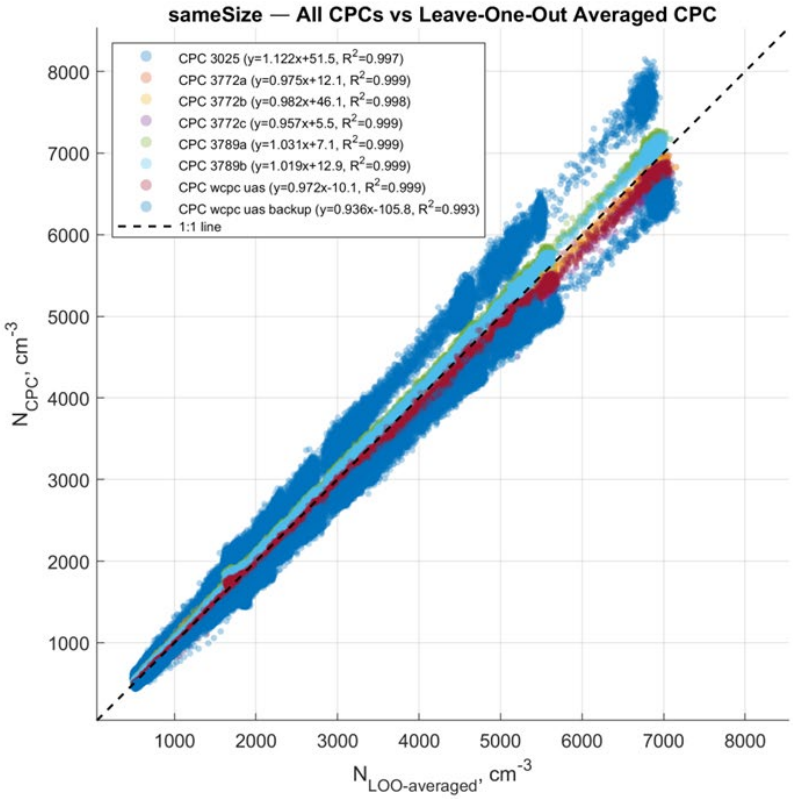


Figure 6. Leave-one-out averaged CPC comparison for the aerosol particles with the same size.

All eight instruments now show R^2 values of 0.993 or higher, with six achieving $R^2 = 0.999$. This represents a substantial improvement over the AE-referenced analysis (where R^2 ranged from 0.977 to 0.983) and confirms that the inter-CPC agreement is excellent when the AE charge-assumption bias is removed. The slopes now range from 0.936 to 1.122, compared to the previous range of 0.736 to 0.860 when referenced to the AE. This confirms that the systematic undercounting observed in the AE comparison was largely an artifact of the multiply charged particle bias in the AE reference, rather than a true deficiency in the CPCs. The intercepts are now dramatically reduced, ranging from −105.8 to 51.5 cm^{-3}, compared to the previous range of 333.8 to 546.2 cm^{-3} in the AE comparison. This indicates that the systematic offsets observed earlier were primarily driven by the AE reference bias.

Note that TSI CPC 3772 units (a, b, c) show slopes of 0.975, 0.982, and 0.957, respectively, with intercepts very close to zero (5.5 to 46.1 cm^{-3}) and R^2 values of 0.998–0.999. The inter-unit consistency remains excellent, with a slope spread of only 0.025, confirming their reliability for deployment. Additionally, TSI CPC 3789 units (a, b) show slopes of 1.031 and 1.019, both slightly above unity, with near-zero intercepts and $R^2 = 0.999$ for both. This indicates they count slightly higher than the group

average, consistent with their lower tunable D50 relative to the CPC 3772 and Magic CPCs. Their inter-unit agreement is outstanding (slope difference of only 0.012).

Magic CPCs (wcpc uas and wcpc uas backup) show slopes of 0.972 and 0.936, both below unity, with the backup unit showing the lowest slope and a notable negative intercept of −105.8 cm^{-3}. While the primary Magic CPC unit performs well ($R^2 = 0.999$), the backup unit shows the weakest agreement in the group ($R^2 = 0.993$, slope = 0.936), suggesting it may require recalibration or maintenance before future deployments.

4.3 Leave-One-Out Averaged CPC Comparison for the Different Size Particles

To evaluate the robustness of the CPC intercomparison across a broader range of conditions, the experiment was extended to include DMA-selected aerosol particles of different sizes, ranging from 30 nm to 180 nm. This "diffSize" test complements the previous "sameSize" analysis by assessing whether the inter-CPC agreement holds across varying particle diameters, which may differentially affect the activation and counting efficiencies of instruments with different D50 cut sizes and condensation mechanisms. The same LOO averaging approach was applied, and the results are presented in Figure 7.

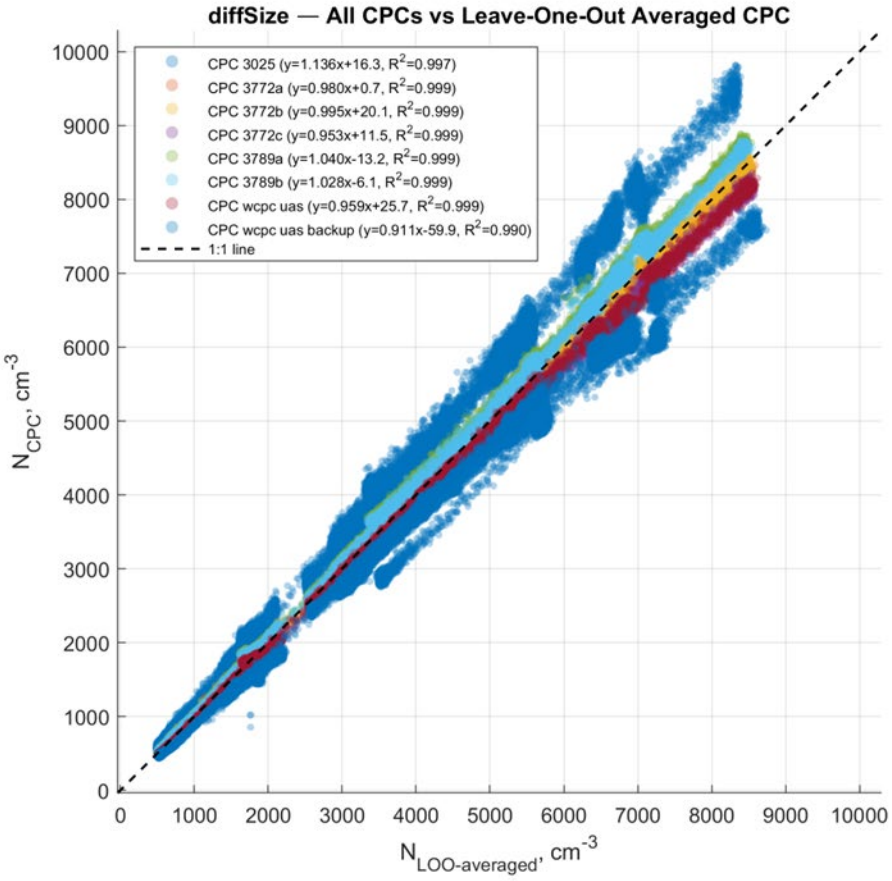


Figure 7. Leave-one-out averaged CPC comparison for the aerosol particles with different sizes.

As shown in Table 4, the LOO analyses of different sizes confirm that the excellent inter-CPC agreement observed in the same-size tests is robust across particle sizes from 30 to 180 nm. All R^2 values remain at 0.990 or higher, with seven of the eight instruments achieving $R^2 = 0.997–0.999$. This demonstrates that the CPCs perform consistently across the typical range of particle sizes.

Table 4. Side-by-side comparison of LOO regression parameters—same size versus different sizes.

Instrument	Slope (Same)	Slope (Diff)	Δ Slope	R^2 (Same)	R^2 (Diff)	Δ R^2
CPC 3025	1.122	1.136	0.014	0.997	0.997	0
CPC 3772a	0.975	0.98	0.005	0.999	0.999	0
CPC 3772b	0.982	0.995	0.013	0.998	0.999	0.001
CPC 3772c	0.957	0.953	−0.004	0.999	0.999	0
CPC 3789a	1.031	1.04	0.009	0.999	0.999	0
CPC 3789b	1.019	1.028	0.009	0.999	0.999	0
Magic CPC uas	0.972	0.959	−0.013	0.999	0.999	0
Magic CPC backup	0.936	0.911	−0.025	0.993	0.99	−0.003

The CPC 3025 slope increased slightly from 1.122 (same size) to 1.136 (different sizes), suggesting that when smaller particles (e.g., 30 nm) are included in the test range, the CPC 3025's lower D50 (~3 nm) provides an even greater advantage over the other CPCs, allowing it to count particles that other instruments may partially miss near their respective activation thresholds.

The three CPC 3772 units showed remarkable stability between the two test conditions, with slope changes of only −0.004 to +0.013. The inter-unit spread remained tight (0.953–0.995), confirming that these instruments are highly reliable and size-insensitive within the 30–180 nm range. Both CPC 3789 units showed a small but consistent upward shift in slope (+0.009 for both units), suggesting marginally improved relative counting efficiency when sampling across multiple sizes. Their inter-unit consistency remained outstanding (slope difference of only 0.012).

5.0 Summary

This report presents a comprehensive intercomparison of nine condensation particle counters (CPCs)—three TSI CPC 3772, two TSI CPC 3789, one TSI CPC 3025, two Magic CPCs (Aerosol Dynamics Inc.), and one Brechtel advanced Mixing CPC (aMCPC)—evaluated against an aerosol electrometer (AE) and against each other using a leave-one-out (LOO) averaging method. The experimental setup employed an atomizer, a DMA, and a residence chamber to deliver well-characterized aerosol through a common sampling manifold to all instruments simultaneously.

Key findings:

1. The Brechtel aMCPC was identified as an outlier and excluded from further analysis due to the flooding problem. It exhibited the lowest R^2 (0.889) and the largest intercept (961.0 cm^{-3}) when compared to the AE. Its removal improved the combined R^2 from 0.9533 to 0.9669, confirming it was a significant source of variance. Further characterization of this instrument is recommended before future deployments.

2. All remaining CPCs systematically undercounted relative to the AE (slopes of 0.736–0.860), likely due to multiply charged particles in the DMA-selected aerosol biasing the AE reference high. This finding has important implications: CPC-consensus references may be more reliable than AE references when the charge state of the aerosol is not well characterized.
3. The LOO analysis revealed excellent inter-CPC agreement. When referenced against the CPC consensus rather than the AE:

   Same-size tests: $R^2 \geq 0.993$, slopes of 0.936–1.122

   Different-size tests (30–180 nm): $R^2 \geq 0.990$, slopes of 0.911–1.136
4. The LOO intercomparison method proved to be a robust and reliable approach, yielding stable results across both same-size and different-size conditions ($|\Delta \text{ slope}| \leq 0.025$ for all instruments). This method is recommended for future CPC intercomparison studies, particularly when an absolute reference may carry its own biases.

6.0 CPC Operation under Lower Pressures

CPCs are often used in environments with significantly lower pressures, such as high-altitude locations or aboard aircraft. Under these conditions, their performance can deteriorate due to changes in saturation profiles and internal particle losses. Research has shown that below 500 hPa, the counting efficiency of CPCs decreases, and the cutoff diameter increases. This is due to the reduced vapor pressure over convex surfaces, which affects the supersaturation criteria necessary for condensation.(Bauer et al. 2023).

6.1 Butanol-Based CPC Performance

A study by Bauer et al. (2023) characterized the pressure-dependent performance of two CPC models: the Grimm 5410 CEN and the TSI 3772-CEN. Their performance was found to be in accordance with the CEN technical specifications at pressures between 1000 hPa and 750 hPa. However, below 500 hPa, both models exhibited a decline in performance, with differences between them. The study included simulations of saturation profiles and calculations of internal particle losses, which reproduced the observed performance decrease and highlighted the impact of the CPC's internal design.

Key behavior trends:

- Above about 750 hPa, the 3772-CEN behaves close to its standard characterization: $d_{p,50}$ near 7–8 nm and plateau efficiency ~100 %.
- Between 750 and 500 hPa, performance is still acceptable for many applications, but you already see a shift in cut-off by a few nanometers and a modest reduction in plateau efficiency.
- Below 500 hPa (375 and 250 hPa), the study reports that both CEN CPCs (TSI 3772-CEN and Grimm 5410-CEN) show clearly degraded performance, with significantly higher $d_{p,50}$ and reduced plateau efficiencies, even though the internal flows and temperatures were kept within reasonable ranges.

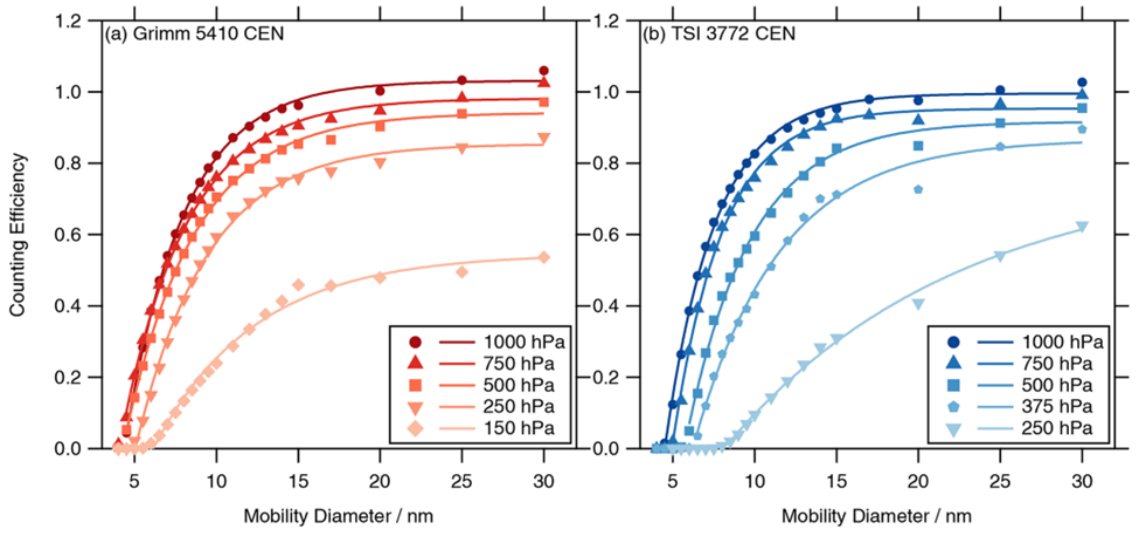


Figure 8. Figure 3 from Bauer's paper: Counting efficiency curves (a: Grimm 5410 CEN and b: TSI 3772 CEN) as a function of the mobility diameter. The counting efficiency was measured with four Grimm CPCs and two TSI CPCs. The markers represent the average over the ensemble of each CPC model. The fit is defined by Equation (3), and the parameters are reported in Table 2 of the paper (Table 5 below).

Table 5. Table 2 from Bauer's paper: Results of the fits from Figures 2 and 3 for the different CPC models and pressure stages. The CPC Faraday cup electrometer (FCE) column is the result of a linear fit through the origin of Figure 2 comparing the concentration of the CPC to the FCE. The η_{plat}, $d_{p,0}$, and $d_{p,50fit}$ columns represent the fitting parameters of the counting efficiency (Equation 3) of Figure 3. The parameters $d_{p,50}$ and $d_{p,90}$ were calculated from the fitted counting efficiency parameters. The edge steepness ε was calculated with Equation (4). A table with the uncertainties of the fits is presented in the Supplement.

CPC model	Pressure (hPa)	CPC / FCE	η_{plat}	$d_{p,0}$ (nm)	$d_{p,50fit}$ (nm)	$d_{p,50}$ (nm)	$d_{p,90}$ (nm)	ε (% nm^{-1})
Grimm 5410 CEN	1000	1.026	1.031	4.4	6.9	6.7	11.8	21.7
Grimm 5410 CEN	750	0.983	0.989	4.0	6.9	6.9	13.9	17.2
Grimm 5410 CEN	500	0.929	0.942	4.3	7.3	7.5	17.7	15.6
Grimm 5410 CEN	250	0.816	0.855	5.0	8.1	8.9	–	12.8
Grimm 5410 CEN	150	0.457	0.546	6.1	10.4	21.5	–	3.2
TSI 3772 CEN	1000	0.986	0.995	4.5	6.6	6.6	11.7	23.8
TSI 3772 CEN	750	0.973	0.953	4.9	7.0	7.2	13.7	21.7
TSI 3772 CEN	500	0.934	0.917	5.7	8.4	8.8	21.6	16.1
TSI 3772 CEN	375	0.831	0.867	6.2	9.8	10.7	–	11.1
TSI 3772 CEN	250	0.549	0.781	8.1	17.9	22.6	–	3.4

6.2 Water-Based CPC Performance

There are no published data or validated simulations for CPC 3789 performance below 200 hPa; The Mei et al. (2021) "simulation-aided characterization" paper explicitly states that measurements and modeling for the vWCPC 3789 were performed only between 500 and 1000 hPa (Hao et al. 2023, Mei et al.,2021).

Given how the 3789 behaves between 500 and 1000 hPa, one can infer the likely direction of change if the CPC is pushed below 200 hPa, but this would be extrapolation, not validated data:

- At 500–1000 hPa, lowering pressure at fixed temperature settings reduces peak supersaturation, narrows the supersaturated region, lowers droplet growth, and decreases counting efficiency; these effects become "significant and larger than 10 %" once pressure drops below about 600 hPa at standard settings.
- Optimizing the conditioner temperature at 500 hPa can restore near-unity plateau efficiency for particles larger than about 15 nm, by increasing the temperature difference and thus the available water vapor.
- Below ~200 hPa, the combination of very low gas density, reduced residence time, and more challenging heat/mass-transfer conditions would almost certainly further reduce achievable supersaturation and droplet growth in the existing 3789 design, unless the hardware (flow rate, temperatures, tube geometry) were fundamentally re-engineered. This is qualitatively consistent with why airborne CPCs for <200 hPa often use different working fluids such as FC-43 instead of water or butanol.

Practical "best-guess" settings by pressure range:

Combining the 2021 and 2023 studies' results yields this practical guidance for the vWCPC 3789 (7 nm mode):(Hao et al. 2023, Mei et al. 2021):

- 900–1010 hPa (near sea level, ground operation):
  - Use factory settings: 30 °C, 59°C, 10 °C. (conditioner, initiator, moderator)
  - This gives high plateau efficiency and design cut-off sizes.
- 700–900 hPa (moderate altitude/slightly reduced pressure):
  - Still acceptable with factory settings, but the onset of degradation appears as pressure approaches ~700 hPa.
  - If you can adjust, a slight reduction of conditioner temperature (e.g., 28–29 °C) while keeping saturator near 59–60 °C increases performance and improves activation of the smallest detectable particles.
- 500–700 hPa (lower troposphere/pressurized cabin):
  - Mei et al. (2021) show that at 500 hPa, 24-27 °C, with a saturator at 60 °C maintains counting efficiency close to 1 for particles >15 nm.
  - The simulations in 2023 indicate that this setting ensures a peak saturation ratio ≥1.3, which they identify as a threshold for good performance under low pressure.

- 300–500 hPa (upper troposphere/aircraft, based on 2023 simulation studies):
  - The 2023 simulation suggests that further lowering conditioner temperature while keeping or slightly increasing saturator/initiator temperature (e.g., 27 °C, 62 °C) can maintain adequate supersaturation even down to tens of kPa (300–400 hPa), but this is based on simulations plus limited experiments and is not a factory-endorsed setting.
- The guiding principle is to choose a temperature pair that yields a saturation peak just above ~1.3; in practice, that means larger temperature differences at lower pressure until you see stable, high plateau efficiency in test measurements.

Below about 300 hPa, the authors still work mostly in simulation space and note that practical airborne use would require careful validation; TSI's own datasheet only guarantees operation down to 75 kPa (~750 hPa), so anything lower is off-specification and must be justified by your own tests.

Table 6. Approximate plateau efficiency of TSI 3789 (7 nm mode) versus pressure with near-optimized conditioner temperature (same initiator and moderator temperatures, 59°C, 10 °C).

Inlet pressure (hPa)	Conditioner temperature (°C)	Plateau efficiency (relative to 1000 hPa)
1000	30	~1.00 (reference)
800	30	~0.98–1.00
700	30	~0.97–0.99
600	27–30	~0.95–0.98
500	24–27	~0.92–0.96
300-400	24-27*	~1.00 (reference)

*Initiator/moderator temperatures are set to 62°C/10 °C.

7.0 Recommendations for Future Deployments

- After this testing, we have implemented the following actions:
  - Recalibrate the Magic CPC backup unit and retest before any field deployment.
  - Investigate the Brechtel aMCPC for potential flow, valve, optical, or firmware issues that may cause the flooding issue.
- Our recommendations for future deployments:
  - Repeat the experimental comparison periodically before the future filed campaign.
  - Extend the intercomparison to lower pressures to evaluate instrument performance at different altitudes, which is particularly relevant for the AAF intended aircraft deployment applications.
  - Characterize the AE multiply charged particle bias quantitatively by comparing AE-inferred concentrations with charge-corrected SMPS data.

- Adopt the LOO method as a standard practice for future multi-CPC intercomparisons to provide a self-consistent, bias-free reference.
- Calibrate the CPCs under the lower pressure to confirm the performance.

8.0 References

Bauer, PS, D Spät, M Eisenhut, A Gattringer, and B Weinzierl. 2023. "Pressure-dependent performance of two CEN-specified condensation particle counters." *Atmospheric Measurement Techniques* 16(19): 4445–4460, https://doi.org/10.5194/amt-16-4445-2023

Bian, JJ, HQ Gui, ZB Xie, TZ Yu, XL Wei, WY Wang, and JG Liu. 2020. "Simulation of three-stage operating temperature for supersaturation water-based condensational growth tube." *Journal of Environmental Sciences* 90: 275–285, https://doi.org/10.1016/j.jes.2019.12.007

Chen, D-R, and DY Pui. 1995. "Numerical and experimental studies of particle deposition in a tube with a conical contraction-laminar flow regime." *Journal of Aerosol Science* 26(4): 563–574, https://doi.org/10.1016/0021-8502(94)00127-K

Hao, W, F Mei, S Hering, S Spielman, B Schmid, J Tomlinson, and Y Wang. 2023. "Mapping the performance of a versatile water-based condensation particle counter (vWCPC) with numerical simulation and experimental study." *Atmospheric Measurement Techniques* 16(17): 3973–3986, https://doi.org/10.5194/amt-16-3973-2023

Hering, SV, GS Lewis, SR Spielman, and A Eiguren-Fernandez. 2019. "A MAGIC concept for self-sustained, water-based, ultrafine particle counting." *Aerosol Science and Technology* 53(1): 63–72, https://doi.org/10.1080/02786826.2018.1538549

Kangasluoma, J, S Hering, D Picard, G Lewis, J Enroth, F Korhonen, M Kulmala, K Sellegri, M Attoui, and T Petäjä. 2017. "Characterization of three new condensation particle counters for sub-3 nm particle detection during the Helsinki CPC workshop: the ADI versatile water CPC, TSI 3777 nano enhancer and boosted TSI 3010." *Atmospheric Measurement Techniques* 10(6): 2271-2281, https://doi.org/10.5194/amt-10-2271-2017

Kangasluoma, J, and M Attoui. 2019. "Review of sub-3 nm condensation particle counters, calibrations, and cluster generation methods." *Aerosol Science and Technology* 53(11): 1277–1310, https://doi.org/10.1080/02786826.2019.1654084

Kerminen, V-M, X Chen, V Vakkari, T Petäjä, M Kulmala, and F Bianchi. 2018. "Atmospheric new particle formation and growth: review of field observations." *Environmental Research Letters* 13(10): 103003, https://doi.org/10.1088/1748-9326/aadf3c

Mei, F, S Spielman, S Hering, J Wang, MS Pekour, G Lewis, B Schmid, J Tomlinson, and M Havlicek. 2021. "Simulation-aided characterization of a versatile water-based condensation particle counter for atmospheric airborne research." *Atmospheric Measurement Techniques* 14(11): 7329–7340, https://doi.org/10.5194/amt-14-7329-2021

Stolzenburg, MR, and PH McMurry. 1991. "An ultrafine aerosol condensation nucleus counter." *Aerosol Science and Technology* 14(1): 48–65, https://doi.org/10.1080/02786829108959470



www.arm.gov

U.S. DEPARTMENT OF
ENERGY

Office of Science